Characterisation of a split gradient coil design induced systemic imaging artefact on 0.35 T MR-linac systems

Louis Marage, Paul-Michael Walker, Julien Boudet, Pierre Fau, Pierre Debuire, Emmanuelle Clausse, Aurélie Petitfils, Léone Aubignac, Stanislas Rapacchi, Igor Bessieres

Characterisation of a systemic artefact on 0.35 T MR-linac systems

Louis MARAGE[1], Paul-Michael WALKER[2], Julien BOUDET[1], Pierre FAU[3], Pierre DEBUIRE[4], Emmanuelle CLAUSSE[5], Aurélie PETITFILS[1], Léone AUBIGNAC[1], Stanislas RAPACCHI[6], Igor BESSIERES[1]*.

[1] Service de physique médicale, Centre Georges-François Leclerc, Dijon, France.

[2] Université de Bourgogne Franche-Comté, Laboratoire Imvia, Dijon, France.

[3] Service de Radiothérapie, Institut Paoli-Calmettes, Marseille, France.

[4] Département de radiophysique, CRLC Val-d'Aurelle-Paul-Lamarque, Montpellier, France.

[5] Groupe Hospitalier Pitié-Salpêtrière, Assistance Publique - Hôpitaux de Paris, Service de Radiothérapie Oncologique, Paris, France.

[6] Université Aix-Marseille, CNRS, CRMBM, Marseille, France.

* Corresponding author: Igor BESSIERES, Centre Georges-François Leclerc, 1 rue Professeur Marion 21000, Dijon, France. Mail: ibessieres@cgfl.fr.

Running title: Systemic artefact on 0.35 T MR-linac

Keywords: MRI, imaging artefact, MR-linac, Split gradient coil.

1 Abstract

Objective: The aim of this work was to highlight and characterize a systemic "star-like" artefact inherent to the low field 0.35 T *MRIdian* MR-linac system, a Magnetic Resonance guided RadioTherapy (MRgRT) device. This artefact is induced by the original split gradients coils design. This design causes a surjection of the intensity gradient in Z (or head-feet) direction. This artefact appears on every sequence with phase encoding in the head-feet direction.

Approach: Basic gradient echo sequence and clinical mandatory bSSFP sequence were used. Three setups using manufacturer provided QA phantoms were designed: two including the linearity control grid used for the characterisation and a third including two homogeneity control spheres dedicated to the artefact management in a more clinical like situation. The presence of the artefact was checked in four different MRidian sites. The tested parameters based on the literature were: phase encoding orientation, slab selectivity, excitation bandwidth (BW_{RF}), acceleration factor (R) and phase/slab oversampling (PO/SO).

Main results: The position of this artefact is constant and reproducible over the tested MRIdian sites. The typical singularity saturated dot or star is visible even with the 3D slab-selection enabled. A management is proposed by decreasing the BW_{RF}, the R in head-feet direction and increasing the PO/SO. The oversampling can be optimized using a formula to anticipate the location of artefact in the field of view.

Significance: The star-like artefact has been well characterised. A manageable solution comes at the cost of acquisition time. Observed in clinical cases, the artefact may degrade the images used for the RT planning and repositioning during the treatment unless corrected.

2 Introduction

The advent of Magnetic Resonance guided RadioTherapy (MRgRT) and the renewed interest for point-of-care low-field Magnetic Resonance Imaging (MRI) systems have brought a whole new generation of designs for MRI magnets and MRI gradients. For the 0.35 T MR-linac MRIdian provided by the Viewray Company[1], the on-board MRI offers improved soft-tissue contrast, daily imaging, intra-fraction real-time and continuous imaging as well as the opportunity for adaptive radiotherapy. However, to accommodate for the linear accelerator (linac) insertion, the magnet and the gradients have been split into two rings. Other applications such as the combination of positron emission tomography (PET) with MRI in PET-MRI systems have also opted for similar designs[2]. The gap imposed in the magnet and the gradient coils in these designs requires compromises in the shape of the gradient coil, which in turn is expected to impact the performance of MRI. In particular, the gradient fidelity, both in time and in space might be degraded[3] as eddy currents arise from the split design with the consequence of a lower general quality of the gradients[3,4], although that can partly be compensated by pre-emphasis[5,6]. The effects can be mitigated using robust 2D Cartesian acquisitions. However, the more demanding MR sequences become, that are already known to require additional corrections[7,8], the more imaging artefacts will arise from these gradient imperfections.

To date, the literature dedicated to the MRI imaging performance of the MRIdian is relatively limited. From a technical point of view, Lewis et al. investigated the image distortion due to the linac components mainly on the balanced steady-state free precession (bSSFP, TrueFISP, T2/T1 weighted) sequence as this is the principal sequence required for clinical use[9]. The occurrence of B1 eddy currents, created by the presence of the linac, has also been investigated, but negligible or minimal effects have been observed on imaging[10–12]. For development purposes, studies have been carried out on other sequences, yet unavailable for clinical work and dedicated, rather, to quantification[13–16]. While the 0.35 T MR-linac is accomplishing its treatment task effectively, unlocking complex treatments possibility for external radiotherapy, the full potential of this device will only be released

with the integration of efficient multi-contrast sequences[17]. However, these sequences are preferably 3D and/or leverage advanced non-Cartesian sampling patterns[13,16], which inherently come with an increased sensibility to gradient imperfection.

In this context, after exposing the hypothesis of the cause and a first view of this artefact, this study will propose a comprehensive characterisation of the artefact. Moreover, management of this artefact was also proposed in the presented work. To our knowledge, this work is the first that describes and characterises an exclusive imaging artefact observed on the MRIdian.

3 Hypothesis

The split gradient system operates a non-bijective gradient intensity in the head-foot direction. The non-bijectivity, in this case, it is a surjection, would not be an issue if the static field fringe was decaying rapidly outside of the spherical field-of-view (FOV). However, the low-field MRI system offers an elongated signal wavelength and an extended sensitivity from coil arrays that can detect signal further from the coil center. The hypothesis of this work is that a unique artefact signal can arise from the combination of three concomitant effects: a/aliasing in the head-foot direction, b/reception from the extended coil sensitivity field and c/ signal compression from the severe split gradient surjection. An explicit visualisation of this artefact is highlighted on the Figure 1., from the clinical-used sequence and a Turbo Spin Echo (TSE) sequence.

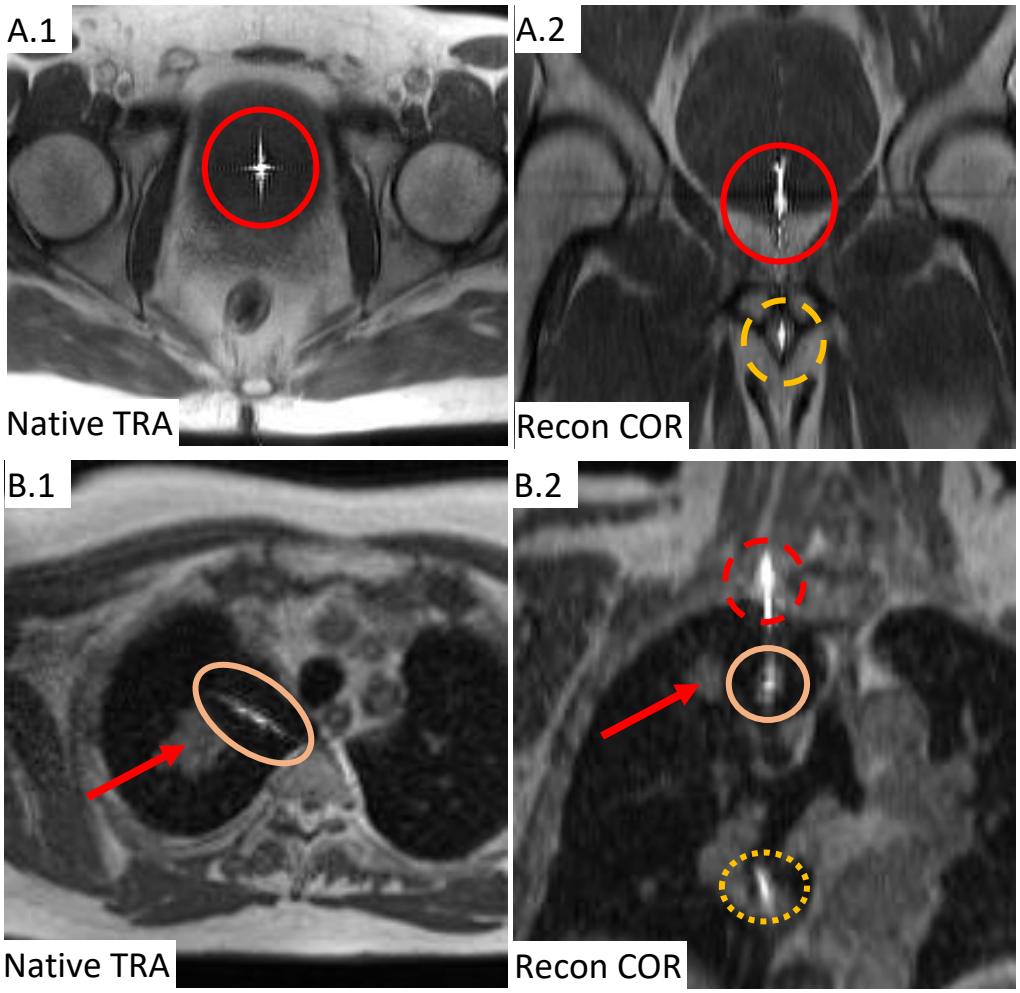

Figure 1. *Row A: a T2 weighted 3D FSE sequence (TR/TE 1800/49 ms, BW 200 Hz/Px, R None, 1 × 1 × 3 mm^3, 64 slices, SO 0%) from a patient in the native axial view (left) and the coronal reconstruction (right). The first "star-like" artefact appeared in the head direction (red circle) and is bigger than the second one which appeared in the feet direction (dashed orange circle). A "zipper-like" artefact bounded the two stars.*

Row B: 25-second acquisition time clinical 3D bSSFP sequence (TR/TE minimum, BW 604 Hz/Px, BW$_{RF}$ high, R 2 PE × 2 3D, 1.5 × 1.5 × 3.0 mm^3, 144 slices, 44.4% SO) in the native axial view (left) and the coronal reconstruction (right). The artefact can be separated into 3 parts, the saturated part near the neck (dashed red circle), a more discrete part near to it in the feet direction (skin color circle) and next to the lung lesion (red arrow) and finally the third part next to the heart (dotted orange circle).

Notably, this artefact can occur when a phase encoding exits in the Z, or head-feet (HF) direction, a signal can be retrieved at a gradient "kink" position and wrapped into the FOV.

The cusp artefact, also called “feather-like”, “annefact” or “startifact”[18], is a candidate that resembles the presented artefact. Actually, their causes are similar. The cusp artefact is caused by a peripheral signal (outside the FOV), excited and encoded as if it were at the isocenter, due to the particular summation of the gradient and the B_0 along the Z direction. Indeed, from the manufacturer’s documentation, the Z gradient shows a “kink” in its linearity as represented in scheme of the Figure 2. However, whereas the cusp artefact occurs on images from TSE type sequences[19], this artefact occurs on every sequence with a phase encoding in the Z direction, thus including 3D axial ones, due to the gradient and B_0 defaults of this design. In short, it could be considered as an artefact combining the cusp artefact and an aliasing artefact. However, because of the elongated receiving field from low-field MRI, the intensity of the aliasing artefact was beyond the regular ones.

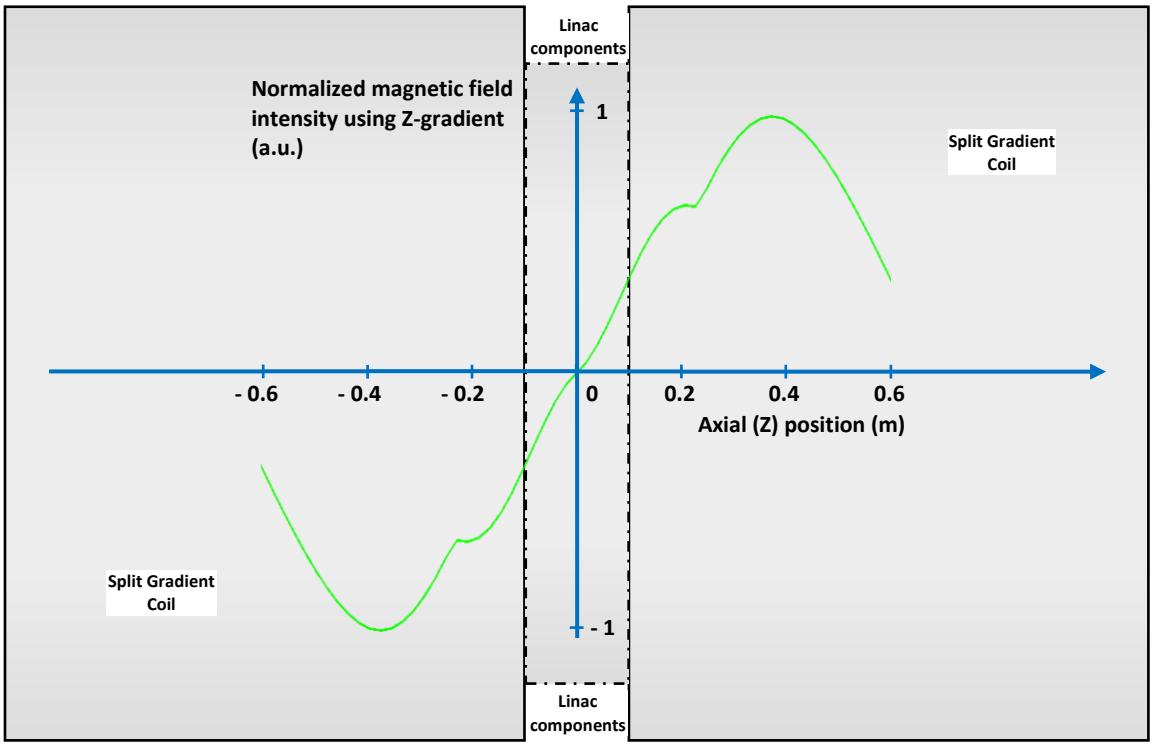

Figure 2 *Simplified scheme of the artefact cause: the unusual gradient non linearity shape in the Z direction. One can see a “kink” in the linearity at +/- 250 mm from the magnetic bore isocenter. Adapted from the Technical user manual, with the permission of Viewray.*

4 Materials and Methods

All acquisitions have been performed on our 0.35 T MR-Linac system (MRIdian, Viewray, Paolo Alto, CA, USA), incorporating a MAGNETOM Avanto system (Siemens Healthcare, Germany)[1]. The images were acquired with the manufacturer-provided 12-channel torso coil array, composed of an array combing two surface flexible coils. Further sequences and finally acquisition parameter variations were carried out in MRI QA mode, i.e. the MRI works in stand-alone mode, without being driven by the Viewray controller.

Even if appearing on every sequence with the right phase encoding direction, as seen on a 3D TSE and 3D bSSFP on the Figure 1., the sequences chosen and used to identify the artefact are 1/ available on every MRIdian to allow easy reproducibility 2/ the simplest possible pulse sequences to avoid confounding factors. Thus 3D true fast imaging with steady-state precession (bSSFP, TrueFISP, T2/T1 weighted), mandatory for clinical routine, and the gradient echo (GRE) Fast Low Angle Shot (FLASH, mostly T1 weighted), were used. The Field Of View (FOV) was standardized to 330 × 330 mm^2 with a 2.5 × 2.5 × 5.0 mm^3 voxel size and placed at the MRIdian's isocenter unless specified otherwise. The 3D distortion correction, or 2D if not applicable, was turned ON for every acquisition. Matching clinical routine, the acquisition box was always locked at this isocenter.

The following acquisition parameters were tested to characterise the artefact, compared to the already referenced artefacts in the literature:

- The slice/slab orientation and phase encoding direction. To check the influence of the X, Y and Z gradients.
- The acceleration factor (R, using the GeneRalized Auto-calibrating Partially Parallel Acquisition (GRAPPA) method) in both phase encoding (R PE) and slab encoding directions in 3D (R 3D). The R value was set to 1 (no acceleration), 2 or 4, with acceleration in on or both directions for 3D sequences, to confront acceleration aliasing with the artifact's aliasing.

- The phase oversampling (PO) /slab oversampling (SO) were varied to change the aliasing position from 7%, to 20% and 30%.
- The slab selectivity was turned ON or OFF, to confront the artefact intensity with respect to excitation outside of the FOV.
- The RF pulse duration, inversely proportional to excitation bandwidth (BW_{RF}). Set to fast (1.28 ms pulse duration, high BW_{RF}), normal (2.56 ms, mid BW_{RF}) and low SAR (3.84 ms, low BW_{RF}) to vary the RF excitation selectivity on potential peripheral signals.

The identification and the management of this artefact was also carried out using the following phantom configurations.

The manufacturer-provided phantoms were used in this study: the Uniformity and Linearity phantom (dimensions $30 \times 30 \times 8$ cm^3) and the uniformity control spheres of 17 and 24 cm diameter. For all imaging sessions, the acquisition FOV was maintained at the isocenter to check the influence of peripheral signals coming from the phantoms thanks to the aliasing.

The Linearity control phantom was first used in the sagittal orientation for explanation purpose (Figure3.A). The grid pattern was placed at the FOV isocenter. A first localizer was acquired in order to check the position, and to perform shimming with the object in the FOV. The later was then sent outside of the FOV to +31 cm in the head direction through a table displacement. The acquisition volume was empty at this step. In this setup, 2D and 3D GRE sequences were acquired in every slice/slab orientation and Phase Encoding (PE) direction. The slab selection was turned off 3D sequences because of the illustrative purpose of this setup using the aliasing to show up the effect of the surjection. This setup will be referred to as the “grid in sagittal setup”.

Following the same set up workflow, the grid was also placed in the axial orientation and its center placed at the isocenter and then sent to +25 cm in the head direction. This setup was used to check the slab selectivity influence on the artefact with the GRE sequence. This setup was also performed in

three other MRIdian sites to check the systemic nature of this artefact. This setup will be referred to as the “grid in axial setup”.

Another setup involved both homogeneity spheres, the 17-cm-diameter one placed at the isocenter and the center of the 24-cm-diameter one spaced at 31 cm in the head-direction at the edge of the pre-amplifier of the torso flexible coil array (Figure 3.B), this last sphere was not included in the acquisition volume this way. The purpose of this setup was to reproduce a “patient-like” configuration, necessary to observe the influence of the BW_{RF} parameters involved in RF selectivity, as well as the effect of the slab oversampling (SO) and the 3D acceleration factor, in a more realistic situation. Thus, the acquisitions were performed used the 3D axial bSSFP sequence as used clinically. This setup will be referred to as the “two sphere setup”. The same experiment was carried out with a conventional 3T MRI for comparison purpose. Details can be found in the supplementary materials.

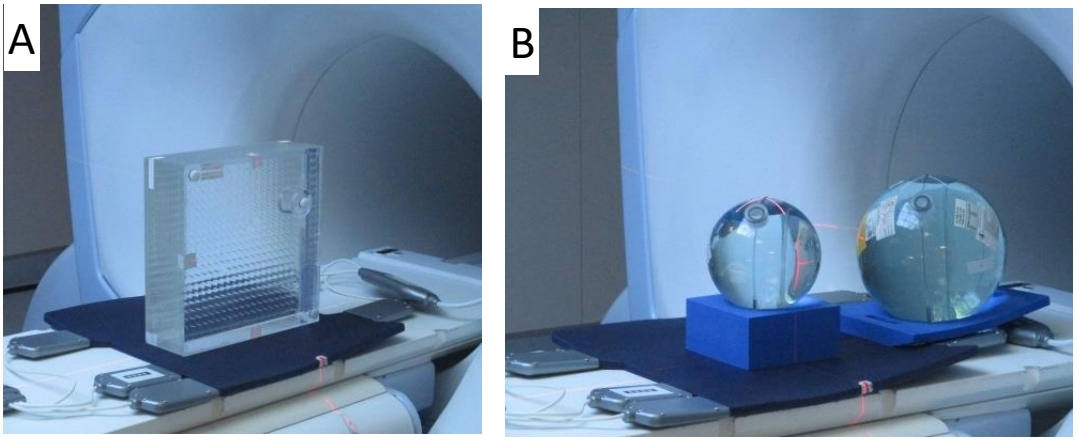

Figure 3. *Pictures of the different phantoms used, the upper torso coil array removed for visibility purpose. A: the linearity control phantom. B: the two spheres setup including the 17 and 24 cm spheres respectively at the isocenter and at 31 cm in head direction.*

The reproducibility of the artefact was checked in three other MRIdian sites.

5 Results

First, no artefact could be observed when a single phantom was placed alone at the machine isocenter, regardless of the sequence used for the acquisition. These experiments confirmed the source of the

artefact coming from peripheral signal. However, the severe distortions can be appreciated thanks to the aliasing when a phantom is placed outside of the FOV, as shown is the figure 4. with the grid in sagittal setup. More precisely it is visible as long as a phase encoding exists in the Z, i.e. head-feet, direction. Only the sagittal with PE in HF direction and the 3D axial views are shown in order not to overload the figure.

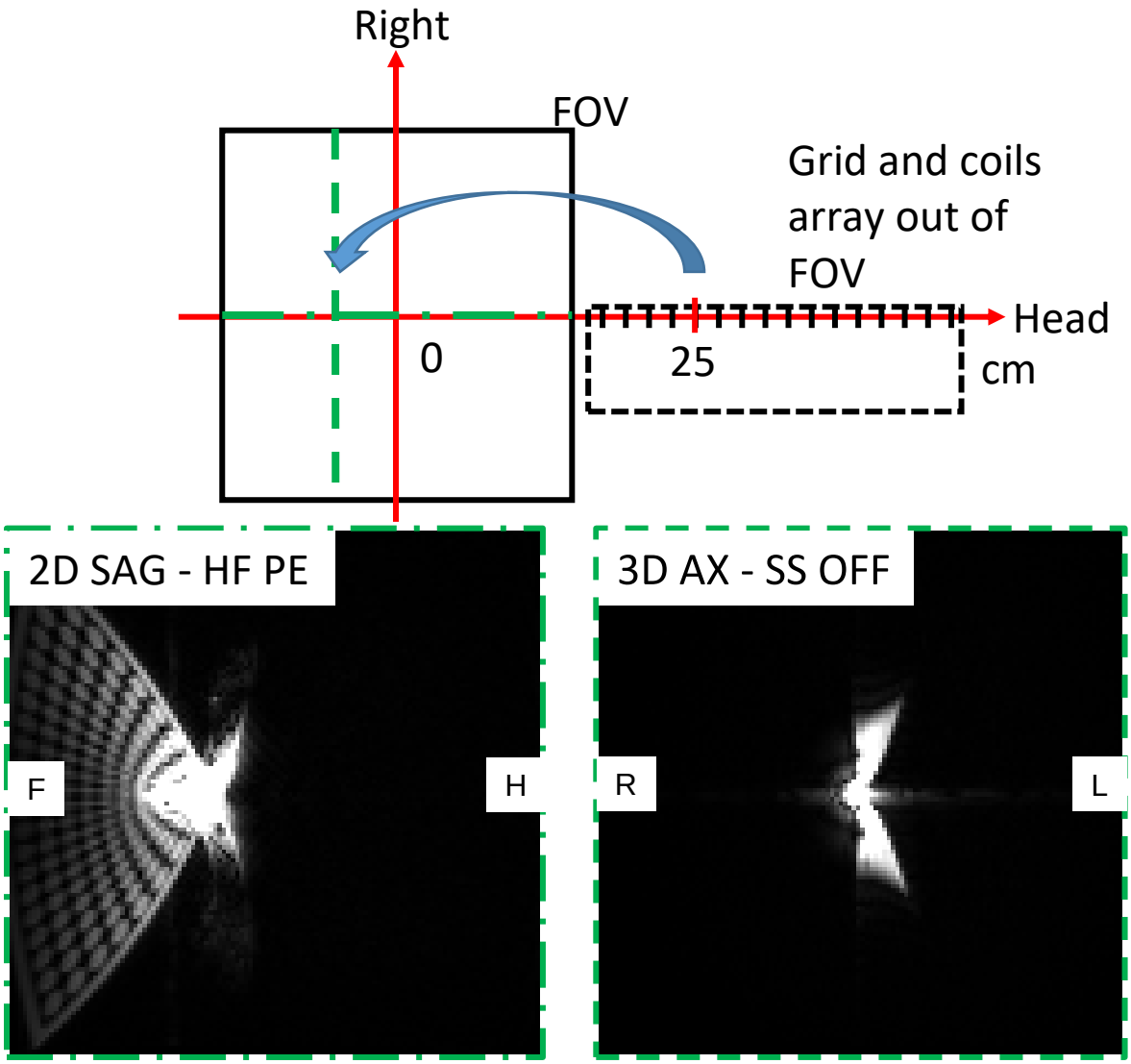

Figure 4*. Top view scheme of the grid in sagittal setup used to understand the artefact and the associated GRE acquisitions: a 2D sagittal with the PE in HF direction (left, dot-dashed contours), and 3D axial without slab selection (right, dashed contours). The aliasing signal of the grid placed outside the FOV is shown here. FOV: Field of View. HF: Head-Feet. PE: Phase encoding. SS: Slab selection.*

Using the grid in axial setup, with the slab-selective excitation disable (Figure 5.A), the shape of geometric distortion of the wrapped grid can be seen. Additionally, an unusual “zipper-like” artefacts is visible in both PE and frequency encoding directions. Only the signal from the “singularity” (central signal saturated dot) became clearly visible with the slab selection turned on (Figure 5.B), the signal from the “regular” distortion and the zipper-like artefacts being mostly suppressed as expected from a slab selection.

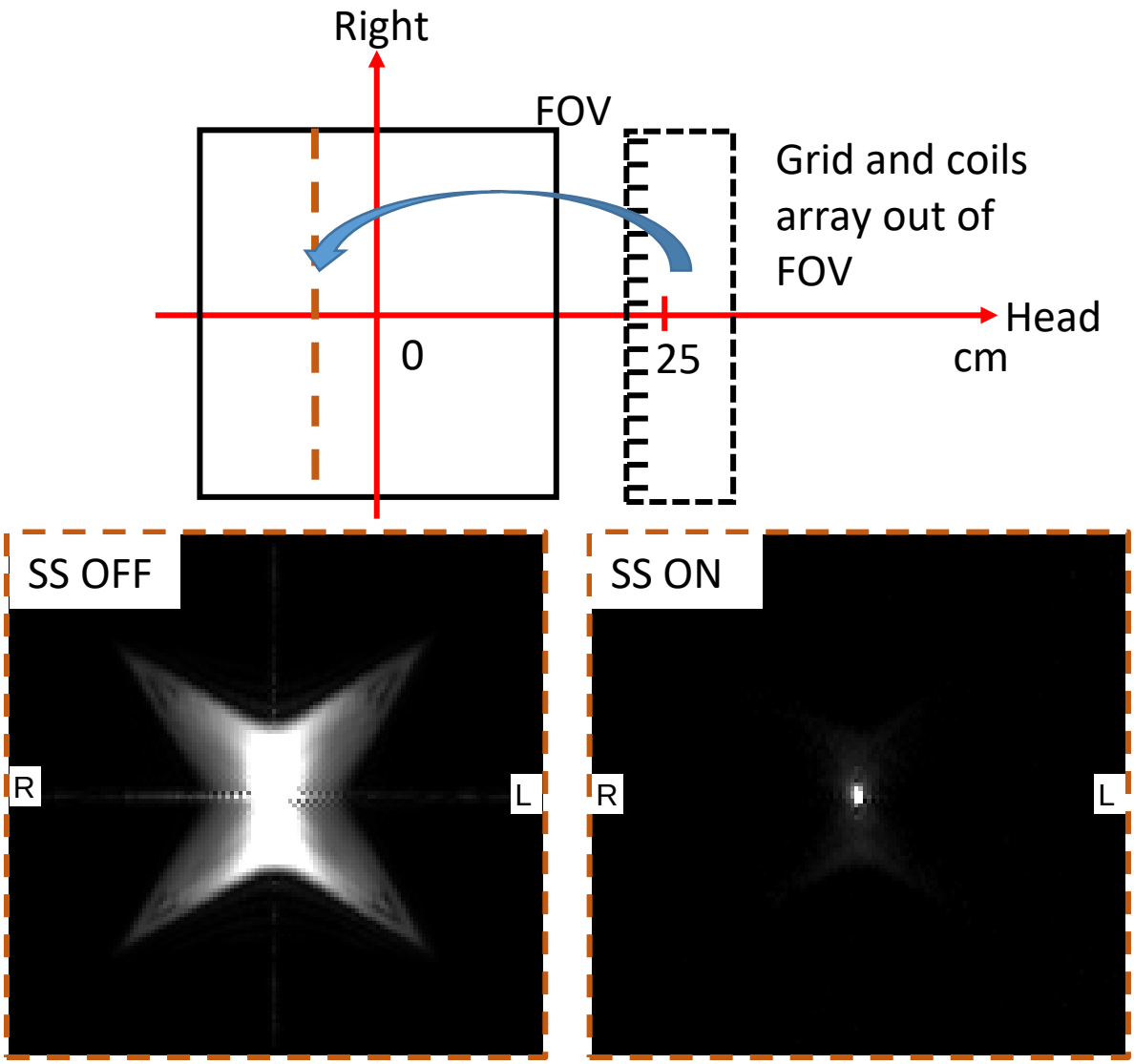

Figure 5*. Top view scheme from the coronal view of the grid in axial setup used to understand the artefact and the associate sagittal image of 3D GRE sequence in axial orientation with (A) and without (B) the slab selection enabled.*

The effects of the RF pulse duration, the R in both in-plane and through plane and the slab oversampling on the artefact can be seen on Figure 6. on the two sphere setup. On these coronal reconstruction images from native axial bSSFP, the influence of the RF selectivity can be seen in the first row of Figure 6. As a reminder, the reception coils was placed at the isocenter. Reducing the BW_{RF} from high to mid, significantly decreased the signal intensity of the artefact. The reduction is less noticeable from mid to low BW_{RF}. For the mid BW_{RF}, the second row shows that the 3D R duplicated the artefact with a noticeable phase inversion and drastically decreased image quality (red arrow). Finally, the third row shows the way to push the artefact into an area that is not reconstructed using the Phase Oversampling (PO) (dashed red arrow). The artefact is not visible anymore with 30% of SO for this FOV. The reproduction of the high excitation RF bandwidth (Figure 6, top right) on a regular 3T MRI, shown in Suppl. Mat. Figure 1, exhibited a significantly different artifact. The two distinctives features of the MR-linac artifact could then be appreciated: a/its abnormal high intensity, and b/the compression of the aliased signal due to the severe and surjective gradient non-linearity.

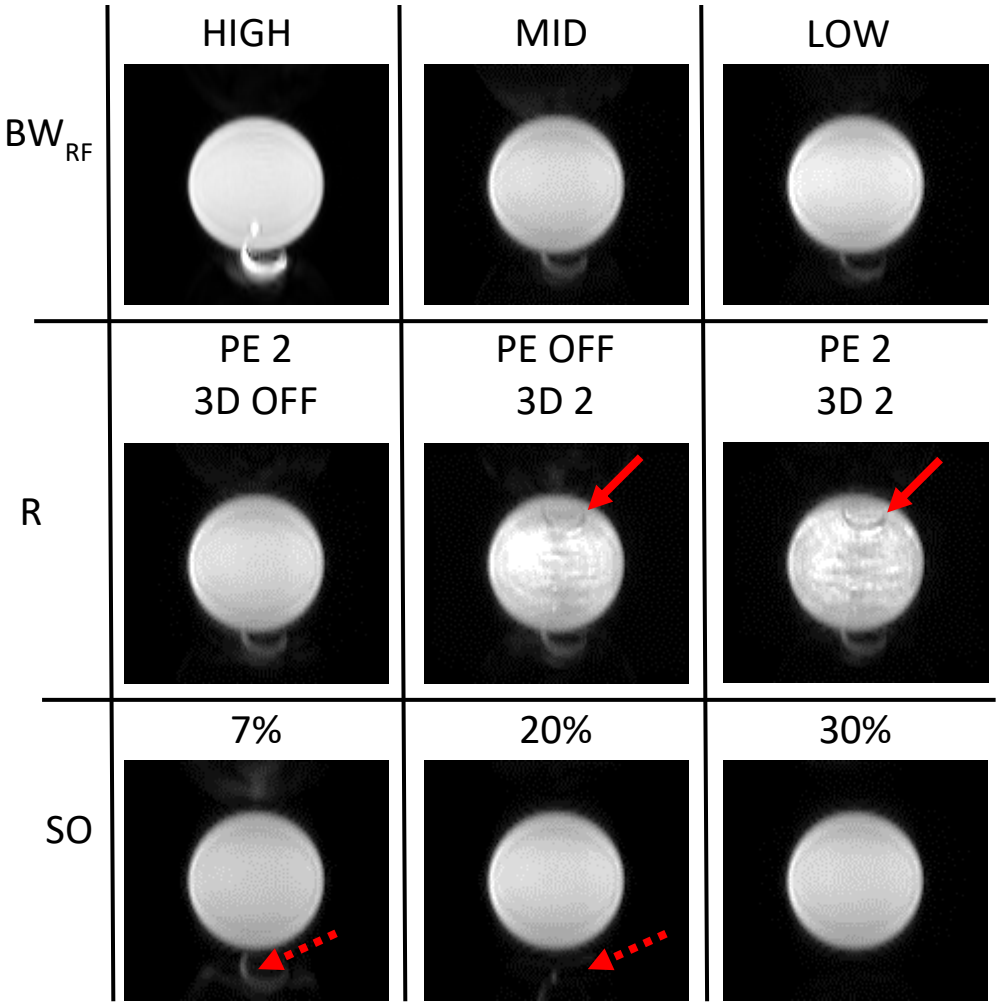

Figure 6. *Coronal image reconstructions from a 3D axial bSSFP acquisition. Except when specified, the sequence parameters are TR/TE minimum, BW 200 Hz/Px, RF Normal, 60 slices, R None, SO 0% and the phase encoding direction were in ante-post and head-feet. BW_{RF}: Excitation bandwidth, R: Acceleration factor, PE: Phase Encoding direction, 3D: Slab encoding direction, SO: Slab Oversampling.*

The optimal SO or PE needed, i.e. artefact invisibility *versus* acquisition time, can be estimated mathematically knowing the position of the Z gradient "kink". This gradient singularity, highly visible in the sagittal orientation using the pattern of the linearity control phantom (Figure 4.), has been localized and stable at 25 cm from the isocenter in both head and feet direction symmetrically. Thus, based on the aliasing artefact mechanism, the localization of the artefact in the FOV relative to the isocenter can be predicted by the following formula:

$$SIF = KP - \left(\left[\frac{KP + \frac{FOV_z}{2}}{FOV_z} \right] \right) * FOV_z$$

SIF being the position of the artefact in FOV, KP the gradient kink position and FOV_z being the length of the FOV in the feet-head direction. This FOV_z includes the oversampling and not only the reconstructed FOV. The brackets indicate an integer division here.

The artefact occurred with excellent reproducibility, i.e. at the same location, on the three other MRIdian installations, tested during our study.

6 Discussion

Our study has highlighted an exclusive star-like artefact seen on the MRIdian system. This artefact was common to four MRIdian systems confirming its systemic nature. A comprehensive descriptive characterisation of the artefact has been carried out. Moreover, several hypotheses about its origin have been explored and confirmed by the experiments described in this study. While this artefact is caused by an extreme gradient-non linearity, it can be differentiated from the regular geometric distortion artefact by its atypical strength producing a saturated pattern. This pattern is robust to the methods that are usually enough to correct the well-known aliasing artefacts like the slab selection.

The descriptive characterisation of the highlighted artefact in this work helped to testify that the unique nature of this artefact is associated with the specificities of the hybrid split gradient coils and the linac design. One can notice that the gantry angle of the linac components was not included in our tests. While the artefact was bound to the Z gradient imperfection, the gantry angle has little to no effect on the artefact visibility. Indeed, Curcuru et al.[11] showed an isocenter shift to x and y directions depending the gantry angle and none in Z direction. These shifts were moreover not visible for the explored resolution here.

However, while the atypical gradient non-linearity in head-feet direction has been explicitly visible on phantoms, it has not been directly measured by a Hall probe neither been fully described by theoretical

modelling. These two points represent the main limits of our study. A full characterisation of the gradients should be undertaken in the future to potentially achieve a direct correction of the artefact. This would represent a step forward for improvements in imaging quality in the MRIdian system. A study on a comprehensive gradient characterisation and correction is currently ongoing for this purpose.

The artefact is easily manageable with some simple changes. The native orientation can be chosen in order to avoid a phase encoding in head-feet direction when it is possible. Otherwise, the management often comes at a cost of time, with compromises such as removing acceleration factor in head-feet direction or adding the right amounts of phase oversampling artefacts, respectively. Therefore, the presence of the artefacts, which has been overseen in the current and clinical usage of the MRIdian system, could be a limit for future imaging applications that could be more sensitive to sequences such as Diffusion Weighted Imaging [9,14] or quantitative MRI protocols needing acquisition times compatible with clinical constraints.

Regarding clinical constraints, the artefact, with hindsight, can occasionally be retrospectively visible on the bSSFP sequences dedicated to the dose planning. Due to the use of an R factor in the Z direction, it mostly appears on the typical rapid thoracic sequences available in clinical mode, sometimes just next to the target volume (Figure 1. Row B.). The quality of the delineation is not impacted according to the expert eye. Besides, while the electronic density map is still calculated from the CT scan, it has no effect on the dosimetry. However, it could be confounding for an inexperienced physician and could spoil a training set for generation of synthetic CT in an MR only workflow perspective.

7 Conclusion

The 0.35 T MR-linac MRIdian system has a known gradient imperfection and we have comprehensively characterised a star-like imaging artefact associated with the split gradient coil design at the origin of this gradient imperfection.

A novel feature of this work is to provide users with management methods to better understand and reduce the visibility of this artefact.

This work will be followed by a complete modelling of the artefacts' behaviour and the gradient imperfection in order to improve further imaging developments on this 0.35 T MR-linac system.

8 Acknowledgements

The authors would like to thank the technicians from Qualimedis involved in this project and the engineer from Viewray for their feedback. The authors also thank the Pr. Hervé Saint-Jalmes for his precious knowledge in the domain.

9 Conflict of Interest Statement

The Centre Georges-François Leclerc has been granted a funding from Qualimedis for the postdoctoral position of Louis Marage.

10 References

1. Klüter S. Technical design and concept of a 0.35 T MR-Linac. *Clinical and Translational Radiation Oncology*. 2019;18:98-101. doi:10.1016/j.ctro.2019.04.007
2. Lucas A, Hawkes R, Ansorge R, et al. Development of a Combined microPET®-MR System. *Technol Cancer Res Treat*. 2006;5(4):5. doi:10.1177/153303460600500405
3. Liu L, Sanchez-Lopez H, Poole M, Liu F, Crozier S. Simulation and analysis of split gradient coil performance in MRI. *Annu Int Conf IEEE Eng Med Biol Soc*. 2011;2011:4149-4152. doi:10.1109/IEMBS.2011.6091030
4. Liu L, Sanchez-Lopez H, Liu F, Crozier S. Flanged-edge transverse gradient coil design for a hybrid LINAC–MRI system. *Journal of Magnetic Resonance*. 2013;226:70-78. doi:10.1016/j.jmr.2012.11.017
5. Boesch Ch, Gruetter R, Martin E. Temporal and spatial analysis of fields generated by eddy currents in superconducting magnets: Optimization of corrections and quantitative characterization of magnet/gradient systems. *Magn Reson Med*. 1991;20(2):268-284. doi:10.1002/mrm.1910200209
6. Wysong RE, Madio DP, Lowe IJ. A novel eddy current compensation scheme for pulsed gradient systems. *Magn Reson Med*. 1994;31(5):572-575. doi:10.1002/mrm.1910310517
7. Jung Y, Jashnani Y, Kijowski R, Block WF. Consistent non-cartesian off-axis MRI quality: Calibrating and removing multiple sources of demodulation phase errors. *Magn Reson Med*. 2007;57(1):206-212. doi:10.1002/mrm.21092
8. Tao S, Trzasko JD, Shu Y, et al. NonCartesian MR image reconstruction with integrated gradient nonlinearity correction. *Medical physics*. 2015;42(12):7190–7201.
9. Lewis BC, Shin J, Quinn B, et al. First clinical experience of correcting phantom-based image distortion related to gantry position on a 0.35T MR-Linac. *J Appl Clin Med Phys*. 2021;22(11):21-28. doi:10.1002/acm2.13404
10. Gach HM, Curcuru AN, Mutic S, Kim T. B_0 field homogeneity recommendations, specifications, and measurement units for MRI in radiation therapy. *Med Phys*. 2020;47(9):4101-4114. doi:10.1002/mp.14306
11. Curcuru AN, Lewis BC, Kim T, Yang D, Michael Gach H. Effects of B_0 Eddy Currents on Imaging Isocenter Shifts in 0.35 T MRI-Guided Radiotherapy (MR-IGRT) System. *Medical Physics*. Published online March 15, 2021:mp.14842. doi:10.1002/mp.14842
12. Michael Gach H, Curcuru AN, Kim T, Yang D. Effects of rotating gantry on magnetic field and eddy currents in 0.35 T MRI-guided radiotherapy (MR-IGRT) system. *Med Phys*. Published online September 25, 2021:mp.15226. doi:10.1002/mp.15226
13. Nejad-Davarani SP, Zakariaei N, Chen Y, et al. Rapid multicontrast brain imaging on a 0.35T MR-linac. *Med Phys*. 2020;47(9):4064-4076. doi:10.1002/mp.14251
14. Lewis B, Guta A, Mackey S, et al. Evaluation of diffusion-weighted MRI and geometric distortion on a 0.35T MR-LINAC at multiple gantry angles. *J Appl Clin Med Phys*. Published online January 15, 2021:acm2.13135. doi:10.1002/acm2.13135
15. Gao Y, Yoon S, Savjani R, et al. Comparison and evaluation of distortion correction techniques on an MR-guided radiotherapy system. *Med Phys*. 2021;48(2):691-702. doi:10.1002/mp.14634
16. Mickevicius NJ, Kim JP, Zhao J, Morris ZS, Hurst NJ, Glide-Hurst CK. Toward magnetic resonance fingerprinting for low-field MR-guided radiation therapy. *Med Phys*. Published online September 18, 2021:mp.15202. doi:10.1002/mp.15202
17. Marage, Bessieres I, Quivrin M, et al. Multi-parametric MRI on a 0.35 T MR-linac: application to prostate radiotherapy treatment follow-up. *In Proceedings of the 31th Annual Meeting of ISMRM, London, UK*. Published online 2022.
18. Graves MJ, Mitchell DG. Body MRI artifacts in clinical practice: A physicist's and radiologist's perspective: Body MRI Artifacts in Clinical Practice. *J Magn Reson Imaging*. 2013;38(2):269-287. doi:10.1002/jmri.24288

19. Rangwala N, Zhou XJ. Reduction of fast spin echo cusp artifact using a slice-tilting gradient: FSE Cusp Artifact Reduction Using Slice Tilt. *Magn Reson Med*. 2010;64(1):220-228. doi:10.1002/mrm.22418